Tribology and Corrosion properties investigation of a Pulse electrodeposition duplex hard-particle-reinforced Ni-Mo nanocomposite coating

Yiku Xu[1*], Mingyuan Fan[1], Yuqing Luo[1], Yongnan Chen[1], Jianmin Hao[1], Xianghui Hou[2]
1 School of Materials Science and Engineering, Chang'an University, Xi'an 710064, Shaanxi, China
2 Faculty of Engineering, The University of Nottingham, University Park, Nottingham, NG7 2RD, United Kingdom

Abstract

In this work, Ni-Mo-SiC-TiN composite coatings were prepared by pulse electrodeposition. Through analyzing the effect of particle content on the phase structure and morphology of Ni-Mo coatings, the relationship between nanoparticles co-deposition amount and the mechanical properties and corrosion resistance of Ni matrix composite coatings was evaluated. The results show that the coating prepared at an electrolyte concentration of 20 g/L is flat and dense presenting the highest particle content. The crystallite size ranging from 28.27 nm to 11.85 nm is affected by different nanoparticle concentrations. As shown by the Tafel polarization and wear test, the incorporation of two hard particles improved the coating performance, and the corrosion current density was reduced by 74% to 1.84 μA/cm^2. The wear rate decreased from 10.196×10^{-4} mm^3/N·m to 2.65×10^{-4} mm^3/N·m, and the average friction coefficient decreased to 0.11. The duplex hard particles play a bearing and hindering role during friction and corrosion. Based on the co-deposition kinetic model, a five-step pulse deposition model referring to nanoparticles was established. It is found that SiC/TiN particles

---

* *Corresponding author: School of Materials Science and Engineering, Chang'an University, Xi'an, 710064, ShaanXi, China*
E-mail address: xuyiku23@hotmail.com

co-deposited to the preferential Ni (111) crystal face and subordinate Ni (200) face. And the good binding ability between the matrix and the nanoparticles results in a high load transfer effect, thus enhancing the tribological properties of the coating. Moreover, the interaction between the duplex nanoparticles was further discussed.

Keywords: Ni-matrix nanocomposite coatings; Pulse electrodeposition; Wear; Corrosion; Duplex particles interaction.

1. Introduction

The development of technology has created high requirements for protective surface coatings of engineering components, such as corrosion resistant and tribological properties. Pure metal or metal matrix coatings prepared by electrodeposition techniques enhances the surface properties of engineering components and applications in automotive, aerospace and many other industrial fields. Metal matrix composite coatings typically contain other metallic elements to form an alloy coating and exhibit better performance than pure metal coatings [1, 2]. Such as the Ni-Mo composite coating prepared by co-deposition molybdenum has good mechanical properties, magnetic properties and corrosion resistance. They also demonstrate the excellent electrocatalytic performance of the hydrogen evolution reaction and exhibit potential as an alternative to chromium coatings [3].

Currently, many nanoparticles are used as a reinforcing phase to improve coating performance [4, 5]. Insoluble particles added to the electrolyte are captured and buried in the substrate coating as the metal ions are reduced during the co-deposition [6, 7].

These particles typically contain ox-ides, carbides, or nitrides, such as SiO_2, Al_2O_3, SiC, TiO_2, Cr_2O_3 and TiN [8-10]. The incorporation of particles of different types, sizes and contents has significant effect on the structure and properties of the coating. Silicon carbide, as one of the ceramic particles, and the Ni-SiC nanocomposite coating has been widely used for its high hardness and excellent tribological properties. [11-17]. Many studies have been conducted on the effects of SiC particle incorporation. The reduction in particle size has a beneficial effect on the comprehensive properties of the coatings [12, 13]. However, it is more difficult for nanosized particles to form composite coatings by co-deposition than micron-sized particles, due to nanosized particles being more easily agglomerated in the electrolyte [14, 15]. Many studies have focused on reducing particle agglomeration and increasing the particle content in the coating by adding suitable surfactants. [16, 17]. Additionally, TiN, as a metal nitride ceramic, has been added to metal-based coatings due to its high hardness, thermal stability, chemical stability, and corrosion resistance [18, 19]. F.F. Xia et al. incorporates TiN nanoparticles into the pure nickel coating using ultrasonic electrodeposition, which revealed that, compared with alloy coating, the incorporation of TiN reduces the porosity of the coating and improves the corrosion resistance of the coating [20].

Concerning various nanocomposite coatings, M. Alizadeh et al. prepared Ni-Al_2O_3-SiC coatings and studied the effect of Al_2O_3/SiC particle content on coatings microstructure and properties. They found that after different contents of nanoparticles were incorporated, the nanocomposite coatings showed prominent and non-uniform morphology. Due to the increase of particle concentration, the nickel crystal structure changed from (100) to (111) and the grain size also decreased significantly. As the content of the two particles changes, the wear rate of the coating decreases, and the corrosion and passivation performance also steadily improves [21-23]. S. Rahemi Ardakani et al. adjusted the concentration of SiO_2 and Al_2O_3 in the electrolyte and obtained the best overall performance of Ni-P-SiO_2-Al_2O_3 coating when the SiO_2 10 g/L and the Al_2O_3 14 g/L are added into the electrolyte. They found that different nanoparticles can promote the co-deposition of each other and the matrix metal so that the prepared nanocomposite coatings have finer grains and denser structures [24]. Zhang et al. added TiN nanoparticles to Ni-W alloy coatings. They showed that incorporation of TiN nanoparticles is beneficial to the (111) orientation of nickel crystals. It increases nucleation rate and limits the growth of grains, which results in the refinement of grains and the uniform growth of Ni-W crystals [25].

As mentioned above, Ni-Mo coatings have broad application prospects and have been extensively studied in recent years. Many studies have focused on the enhancement of Ni-Mo coatings by different types of particles. [26, 27]. In previous works, direct-current electrodeposition was used to successfully prepare Ni-Mo-SiC-TiN nanocomposite coatings. The incorporation of two kinds of hard particles improved the comprehensive properties of metal coatings [28]. In this work, Ni-Mo-SiC-TiN nanocomposite coating was prepared at different particle concentration by pulse electrodeposition. The phase structure, morphology, chemical composition, tribological properties and corrosion resistance of coatings under different nanoparticle contents were studied. The mechanism of the action of nanoparticles in coatings was studied.

2. Experiment

2.1. Fabrication of Ni-Mo-SiC-TiN nanocomposite coatings

Ni-Mo coating and Ni-Mo-SiC-TiN coatings were prepared by pulse electrodeposition. The material used for the anode is a pure nickel (99.99%) plate, and 6061 aluminum alloy plates (20 mm×20 mm×3 mm) were used as the cathode. All samples should be pretreated before use, and the surface shall be mechanically polished to 1500-grit finish and then degreased in 0.21 M Na_2CO_3, 0.13 M Na_3PO_4, and 1.8 M NaOH at 55 °C for 2 min and then activated in 4.76 M HNO_3 for about 4 min at room temperature. After activation treatment, the substrate was rinsed and put into zinc bath for 1 minute. The zinc bath compositions were 0.5 M ZnO, 0.007 M $NaKC_4H_4O_6 \cdot 4H_2O$, 12 M NaOH, and 0.006 M $FeCl_3$. This pretreatment process could effectively improve the bonding ability of the coatings to the substrate. The nanoparticles were mixed with distilled water, which was ultrasonically dispersed for 3 hours, and mechanically stirred for 12 hours to prevent the agglomeration of nanoparticles. Then, the nanoparticle slurry is mixed with the electrolyte. The average size of SiC and TiN nanoparticles (purity> 99.9%) was about 40 nm and 20 nm, respectively. The electrolyte is composed of analytical reagent and nanoparticle slurry, the same amount of SiC and TiN particles are added each time. Table 1 list the detailed composition of the electrolyte and the electrodeposition operation parameters. The distance between the anode and the cathode was set to be 4.0 cm. At constant temperature, magnetic stirring at 350 rpm during electrodeposition. The prepared samples were rinsed with deionized water.

2.2. Characterization of Ni-Mo-SiC-TiN nanocomposite coatings

The surface morphology and cross-section morphology of various samples were obtained and analyzed using Hitachi S-4800 FE-SEM (Field Emission Scanning Elecrton Microscopy). The instrument is equipped with an energy chromatograph (EDS) for qualitative and quantitative analysis of constant elements in the micro area of the sample.

The coating samples were subjected to Bruker D8-advanced X-ray diffraction, The diffracted conditions were as follows: Cu-Kα radiation, scan rate of 0.3 °/min and 2θ range is 20°~80°) to detect the phase identifications. Crystallite size (D) is calculated by Scherrer relation:

$$D = \frac{k\lambda}{\beta cos\theta} \tag{Eq.1}$$

where K is 0.89, λ is 0.154056 nm, θ and β corresponds to the Bragg angle and full width at half maximum(radian) of the characteristic peak respectively

The structure of the coating and the existence of nanoparticles were further characterized by transmission electron microscopy (FEI Talos F200X TEM).

The 3D morphology of the surface and the coating after the wear test were observed by a laser scanning confocal microscope OLS4100 (LSCM).

The Vickers microhardness for composite coatings was measured using microhardness tester (HV-1000A). The load is 20 g and the holding time is 10 s. Microhardness measurements were performed on polished cross-section. The average of seven measured values was selected as the reported value. The friction and wear properties of the coating were evaluated at room temperature and dry condition by pin disk wear machine (MMQ-02G). GCr15 bearing steel balls (6 mm diameter) used as the abrasive. The test was performed for 20 minutes under a load of 4 N, a friction radius of 3 mm, and speed of 100 r/min. After the test samples were ultrasonically cleaned, the masses before and after wear were weighed with an analytical balance. S4800 FE-SEM was used to observe the surface morphology of the worn samples and analyze the wear mechanism.

The corrosion behaviors were tested through a three electrode working system. Prepare 3.5 wt% NaCl solution as corrosion medium. The saturated calomel electrode is the reference electrode, and the platinum electrode is the counter electrode. The effective area exposed by the sample was 1 cm^2. The sample needs to be immersed in the corrosion solution for 30 minutes to keep the open circuit potential stable. The dynamic potential polarization scan rate is 1 mV/s, and the scan range is -1 V and +1 V. The corrosion potential (E_{corr}) and corrosion current density (i_{corr}) were determined by Tafel extrapolation. The corrosion morphology of the coating was characterized by SEM.

3. Results and discussion

3.1. Surface morphology

Surface micrograph of Ni-Mo (a, b) and Ni-Mo-SiC-TiN nanocomposite coatings (c-h) are shown in Fig. 1. The as-prepared Ni-Mo coating has a pyramidal structure with binary symmetrical grains. As incorporation of duplex nanoparticles in the Ni-Mo coatings, the surface topography develops from pyramidal to spherical. The coatings with relatively low particle concentrations of 4 g/L and 8 g/L showed a rougher surface, which is attributed to the fewer nucleation sites for nickel grains served by SiC/TiN nanoparticles during the electrodeposition process. With the increase of nanoparticle concentration, the coating surface becomes smoother and the grain size of the prepared coating synchronously decreases. As the nanoparticle concentration reaches 20 g/L, the coating surface becomes almost flat without obvious protrusions.

Fig. 2 indicates the LSCM 3D morphology of coatings further demonstrates the effect of nanoparticle content on coating roughness. In the absence of particles, Ni ions are uniformly deposited and grown on the substrate, which can be confirmed from the flat surface of the Ni-Mo coating. The coating prepared at 8 g/L has a peak of more than ten microns. With the increase of particle concentration, the coating gradually smooth, eventually the surface prepared at 20 g/L exhibiting a flat feature. The surface roughness of the Ni-Mo coating is 3.2 μm. In contrast, the incorporation of nanoparticles affects the roughness from 9.8 μm (with 8 g/L SiC/TiN), 5.6 μm (with 16 g/L SiC/TiN) to 3.7 μm (with 20 g/L SiC/TiN). This indicates that high concentration nanoparticles provide more nucleation sites, which inhibits the growth of Ni grains, accompanied by the nanoparticles dispersing evenly on the coating surface.

The cross-section micrographs of the composite coating prepared are shown in Fig. 3. All the deposited coating is uniformly dense. No discontinuities and cracks at the interface, which clearly showed a good bond. From the cross-sectional micrographs, the effect of the incorporation of different particle contents on the roughness of the coating can be clearly observed. The high-magnification SEM cross-sectional micrographs in Fig. 3 shows that the nanoparticles deposited in the coating and their distribution. In addition, compared with the Ni-Mo thickness of 10.15 μm, the incorporation of the particles changed the thickness to 14-17 μm. This can prove on one hand that the incorporation of particles promotes the deposition of the Ni coating.

3.2. Analysis of Coating Structure

Fig. 4a presents The XRD patterns of SiC and TiN powders. The characteristic peaks of the two particles, such as for (111), (200), (220), and (311) are consistent with PDF number: 75-0254, number: 87-0628. Fig.4b exhibits the XRD spectra of the nanocomposite coatings, the three peaks of typical Ni coatings appearing on 44.36˚, 51.59˚ and 76.08˚ correspond to Ni (111), (200), (220) crystal planes respectively (PDF number: 87-0712), and (111) preferential crystal orientation occurring obviously. As molybdenum replaces part of the lattice of nickel and forms a solid solution of the FCC structure, the diffraction peak of Mo does not appear [28]. Consistent with our former research, the characteristic peaks of the two nanoparticles were not detected at low concentration. The main peaks of SiC and TiN were detected through the addition of particles in the electrolyte at 20 g/L and more.

It should be concerned that as the content of SiC and TiN in the electrolyte increases, the diffraction peaks are gradually broadened, particularly the preferential (111) diffraction peak. As reported, this is related to both microstrain and grain size [29]. While, the microstrain caused by the electrodeposition sample is rather small [30], and studies have shown that the addition of nanoparticles can reduce the grain size of the coating matrix [31, 32]. With the raise of the SiC/TiN concentration, many nucleation sites on the cathode surface increased, meanwhile the growth of Ni crystallites was suppressed, thereby achieving grain refinement. The grain sizes of different Ni-Mo-SiC-TiN nanocomposite coatings calculated using the Scherrer equation are shown in Fig. 4c. Compared with the average Ni-Mo coating grain size of 28.27 nm, the average grain size of the nanocomposite coating obviously decreased to 11.85 nm with the concentration of 20 g/L.

For better understanding the reinforced coatings, the weight percentage of Mo and SiC/TiN particles incorporated in the coating is also calculated and displayed in Fig. 4d. In the Ni-Mo matrix nanocomposite coating prepared at different particle concentrations, the content of molybdenum changed slightly in the range of 12-13 Wt%. With the increase of particle concentration, Ni content gradually decreases. Compared with the alloy coating Mo/Ni ratio of 0.123, the addition of nanoparticles increased the Mo/Ni ratio to 0.168. This may indicate that nanoparticles promote the co-deposition of Mo. The particle content in the coating increases with the presence of more nanoparticles in the electrolyte, reaching a peak at a concentration of 20 g/L (10 g/L SiC+10 g/L TiN). It is worth mentioning that although the concentration of the two particles in the electrolyte is equal, the deposition amount of TiN particles is always greater than SiC particles. This phenomenon can be attributed that the more activation of TiN is than SiC during the co-deposition, which may be related to the wettability of the two nanoparticles, conductivity, Zeta potential, and their interaction with Ni ions [33].

Fig. 5 displays the TEM bright-field image of Ni-Mo-SiC-TiN (20 g/L) nanocomposite coating. The EDS mapping indicates the existence of two types of nanoparticles passes through the distribution of Si, C, Ti and N elements. The presence of nanoparticles are considered to be the aggregated parts of bright spots in the corresponding element map.

3.3. Tribological behavior of coatings

As demonstrated in Fig. 6a, the microhardness of the Ni-Mo coating is 386 HV, and the addition of nanoparticles from 4 g/L to 20 g/L increased the microhardness of the coating from 431 HV to 561 HV. The hardness increase has been attributed to two factors: grain refinement of the matrix coating and reinforcing phase induced hardening (related to the Orowan mechanism) [34, 35]. According to Hall-Petch equation, the grain size is inversely proportional to the microhardness, which is consistent with our experiment results as Fig. 4c exhibited. Meanwhile, the more particles in the coating, the smaller average distance λ between uniformly dispersed particles. The dislocation lines do not easily bypass the particles, which enhances the composite coating strengthening.

Wear tests performed on coatings with different nanoparticle content, indicate that the Ni-Mo coating exhibits a continuous increasing friction coefficient and attains a maximum value of approximately 0.35(Fig. 6b), which can be caused with the severe plastic deformation at low hardness, adhesion and delamination. The friction coefficient of the coating prepared at 4 g/L still performed fluctuating and unstable to the high spacing of the particles during co-deposition at low nanoparticle concentrations, which does not produce sufficient dispersion strengthening. Therefore, the instability caused by the stress applied at the interface between the particles and the substrate may cause the particles to fall off. Since the increase of particle content in the coating led to more stable the friction coefficient, the Ni-Mo-SiC-TiN coating deposited at 20 g/L demonstrates the lowest friction coefficient, about 0.11. Moreover, the dispersion strengthening also made the friction coefficient more stable.

The wear rate is also proved to decrease as the particle content increases, as shown in Fig. 6a. Compared to 10.196×10^{-4} $mm^3/N.m$ of Ni-Mo coating, the wear rate of the coating prepared at 20 g/L decreased to a minimum value of 2.65×10^{-4} $mm^3/N.m$, a reduction by about four times. But the wear rate rised after the concentration of nanoparticles exceeded 20 g/L.

Fig. 7 displays the wear surface of Ni-Mo matrix nanocomposite coatings with different particle contents. The wear track of the Ni-Mo coating in Fig. 7a possessed a severe wide peeling along the sliding direction, due to the low hardness of the coating. Therefore it is not hard to understand high plastic deformation and adhesive wear were caused by the combined action of compression and shear stress during the wear process. With the incorporation nanoparticles concentration of 8 g/L (Fig. 7b), micro-cracks still exist on the surface of the wear, and significant stress concentration occurs at the interface between the hard nanoparticles and the soft coating. There are strong signs that the incorporation of nanoparticles changed the wear morphology prominently. As seen that the increasing particle concentration decreased the width of the wear track, and both surface peeling and plastic deformation were significantly reduced. It is indicated by the emerged wear grooves that the wear mechanism of the coating changes to abrasive wear, which proves the better wear resistance of the nanoparticles coatings. The wear depth is described by the 3D morphology of the worn surface. The decrease of wear depth can be seen from the record of wear track by LSCM data, which can reflect the friction performance of the coating.

Fig. 7d exhibiting the coating prepared at 20 g/L shows that the surface roughness of the prepared coating was not completely eliminated after wear. This may be due to insufficient plastic deformation of the coating under a low load of 4 N. When continuing to increase particles in the electrolyte, the slight increase of wear rate can be attributed to the relationship between coating structure and nanoparticle content. It can be seen from Fig. 1h that when compared with the coating prepared at 20 g/L, the surface is slightly rough and more prominent. In the process of wear, the stress concentration in the protruding part leads to more coating peeling. In addition, according to Fig. 4d, when the particle concentration is saturation, the decrease of the content in the coating may also lead to the increase of wear rate.

As stated above, the coating deposited at 20 g/L has the best wear resistance. The change in the abrasion resistance of the coating can be essentially attributed to the structural changes caused by the addition of particles. As the wear schematic shown in Fig. 7e, fatigue cracks caused by high stress along the sliding direction accelerate the peeling of the Ni-Mo coating. The two as-deposited hard nanoparticles in the composite coating could prevent the shape deformation through suppressing dislocation motion. The evenly distributed nanoparticles reducing the damage of steel ball to the matrix coating, definitely play a bearing role during the wear process.

3.4. Anti-corrosion capability of the coating

The corrosion resistance of the coatings prepared at different particle concentrations was tested for polarization in NaCl solution. Fig. 8a shows the potentiodynamic polarization curves for Ni-Mo-SiC-TiN coatings. And Table 2 lists the β_a, β_c, I_{corr} and E_{corr} calculated from the anode and cathode intersections of the Tafel curve using Tafel extrapolation. Polarization resistances (R_p) calculated using Stern-Geary relationship equation:

$$R_p = \frac{(\beta_a \times \beta_c)}{2.303 \times i_{Corr}(\beta_a + \beta_c)} \quad \text{(Eq.2)}$$

Compared with the corrosion potential of Ni-Mo coating at -0.394 V, the incorporation of nanoparticles makes the corrosion potential move in a positive direction from -0.361 V to

-0.250 V with the increase of nanoparticle content. The current density decreases from 6.96 μA/cm^2 to 1.84 μA/cm^2 with the concentration of SiC and TiN from 0 to 20 g/L. Polarization resistance increases to a maximum value of 3887 Ω·cm^2 at 20 g/L. As the SiC and TiN concentration increased to 24 g/L, the I_{corr} was increased to 2.01 μA/cm^2.

The reinforcing phases, microstructure, and crystallite size of the coating can affect the corrosion resistance [36]. As inert particles, SiC and TiN play a positive role in the isolation and hindrance of corrosion medium. As physical barriers, the uniformly distributed particles can effectively reduce the contact area of the metal coating in the corrosive environment and thus inhibit the corrosion. In addition, the electrochemical mechanism is another factor affecting the corrosion resistance of coatings. The micro-galvanic cells formed at the interface between the nanoparticles and the matrix affects the corrosion behavior of the coating. When the sample is immersed in the corrosion solution, the electrochemical potential of SiC and TiN is more positive than that of the Ni matrix. Therefore, the nanoparticles play the role of the cathode and metal coating as the anode. Compared with nickel, the electrochemical potential of SiC and TiN is higher [18, 37]. The formation of micro-galvanic cells was beneficial to anodic polarization, which promotes the passivation process of nickel and reduces the corrosion rate of the nickel matrix in the NaCl corrosion medium.

The morphology of nanocomposite coatings after polarization experiments are shown in Fig. 8b-e. The coating on the surface of the alloy provides effective protection. Comparing the coating with different samples, corrosion cracks, and corrosion products occur on the surface of a Ni-Mo coating. As more particles presenting in the coating, the corrosion defects decrease. The coating prepared at 20 g/L nanoparticle concentration was compact and uniform, with no obvious corrosion characteristics. In the process of electrodeposition, SiC and TiN particles can occupy some cracks and voids in the coating. The size of these defects is about micrometers, and the location of the defects is easier to be corroded. Therefore, particles smaller than 100 nm are more likely to occupy defects. The existence of nanoparticles inhibits local corrosion, mainly uniform corrosion, and the particles as corrosion barriers can effectively prevent the further expansion of corrosion holes [36, 38]. As the concentration of particles in electrolyte continues to increase, the content of nanoparticles decreases. The formation of voids on the surface is shown in Fig. 1h. When the corrosion solution enters the defect position, the corrosion resistance of the coating may be reduced.

3.5. Discussion of Co-deposition model and duplex particles interaction

Several co-deposition models have been proposed, such as the Guglielmi model [39] and Celis model [40]. Guglielmi proposed that the non-conductive nanoparticles suspended in the electrolyte must be adsorbed by two consecutive steps. First step, outside the dense layer of the cathode, particles are surrounded by ions to form reversible weak adsorption. Then, the weakly adsorbed particles take off the surface, with a strong adsorption of ions, and the nanocomposite coating is embedded by the growing metal. Celis model includes a five-step mechanism that comprehensively considers fluid mechanics and interfacial electric field factors. To better describe the incorporation of particles in pulse co-deposition, based on the above two models, a modified five-step model is gained and described in Fig. 9g. The steps include: (ⅰ) metal ions form an adsorption layer on the particle surface, (ⅱ) the charged particles pass through the diffusion layer through convection and diffusion, and reach the boundary of the electric double layer, (ⅲ) charged particles are adsorbed on the cathode, (ⅳ) the cation diffuses and discharges on the surface of the electrode or particle, and (ⅴ) with the nucleation and growth of the matrix, the nanoparticles are buried in the coating. In the embedding stage, Ni ions reduce at the particle/cathode interface until the whole surface of the particles is covered by Ni atoms. [41].

Fig. 9a shows the more detailed study of the structure of the co-deposited Ni-Mo-SiC-TiN composite coating at 20 g/L by TEM. The selected area electron diffraction (SAED) pattern containing (111), (200), (220) and (311) crystal planes represents the Ni-Mo solid solution matrix with a face-centered cubic structure (Fig. 9b). As-deposited SiC particle determined by SAED as Fig. 9c exhibited, demonstrates the space group was F-43m with a lattice constant of 4.348 Å. And Fig. 9e depicts the fast Fourier transform (FFT) of the deposited TiN particle with a space group of Fm-3m and a lattice constant of 4.244 Å.

In the process of composite electrodeposition, Ni^{2+} in the nickel sulfate electrolyte existing in the form of $Ni[(H_2O)_6]^{2+}$ is known to be with excellent stability. Once hard ceramic particles are added as the second phase particles, the metal ions can reach the cathode in two different ways. The metal ions either directly reach the cathode through convection/mass transfer, or reach the cathode together with the particles [42]. The electrical conductivity of the particles can consequently influence the co-deposition. The particles with poor conductivity are gradually embedded by metal, while for the particles with good conductivity, the matrix metal will rapidly grow on the surface of the particles and surround them [43, 44]. TiN particles with high conductivity can rapidly embed into the metal matrix during deposition, which increases the effective area of metal ion discharge and reduction on the cathode. Ref. 45 has reported that SiC has poor electrical conductivity, and TiN as a kind of particles with good electrical conductivity is often used to improve the performance of SiC-based ceramics. In the mixed electrolyte mixed with many kinds of nanoparticles, more conductive particles enhance the co deposition of non-conductive particles [46]. In this work, the clear interface between the TiN particles and the Ni matrix was captured in Fig. 9f, voids and harmful interface reactants were not detected. The crystalline plane spacing was obtained by measuring five lattice distances. The plane fringes of 0.203 nm and 0.211 nm are distributed to the two planes of Ni (111) and TiN (002), respectively. As demonstrated in the study, both alloy coatings and nanocomposite coatings exhibited a preferential growth on the crystal face (111). It is very common to find SiC and TiN nanoparticles co-deposited to this preferential Ni (111) crystal face, but also a certain extent on the subordinate Ni (200) face. Compared the nanoparticle size of 20/40 nm with the composite coating grain size of 11.85 nm, it is deduced that the duplex nanoparticles deposited randomly to the matrix crystal faces during the pulse electrodeposition process. In particular, the good binding ability between the matrix and the nanoparticles results in a high load transfer effect, thus enhancing the tribological properties of the coating [47].

The incorporation of conductive SiC/TiN nanoparticles also caused the formation of protruding clusters in the coatings. The mechanism is sketched in Fig. 9h. Under the premise of relatively flat surface and the actual current density equals to the average, the unit cell grows uniformly due to the same growth rate. Otherwise, the producing protrusions of conductive particles on the cathode surface as conductive high spot, will definitely cause non-uniform deposit rate. The reduction reaction of ions causes the nickel atoms to nucleate at these protrusions positions and continues to grow preferentially so that a raised cluster structure is formed, as seen in Fig.1. In addition, these protrusions have the same charge in the electric field, and the repulsive force between them ensures the vertical growth and then forms a large protrusion cluster [48, 49].

We also find that the duplex SiC/TiN particles can interact each other and promote the total deposition amount. As shown in Fig. 4d, the SiC/TiN content of the coating prepared at the particle concentration of 20 g/L reaches the maximum value. When particles added in the electrolyte increase, more nanoparticles can pass through the diffusion layer to the electric double layer. Especially under the action of the electric field and the effect of the interface field, particles fixed on the surface of the cathode can be definitely improved. Therefore, as a kind of particles with good electrical conductivity, TiN can effectively improve the performance of SiC to achieve a promoted co-deposition into the Ni-Mo composite coatings.

4. Conclusion

In the study, duplex hard-particle-reinforced reinforced Ni-Mo nanocomposite coating was prepared by pulsed electrodeposition. The effect of SiC/TiN concentration in electrolyte on the preparation of coating was studied as follows:

The addition of nanoparticles changed the surface morphology from a pyramid structure to a spherical structure. As the particle concentration increased to 20 g/L, the coating deposited was the most uniform and flat with the highest nanoparticle content. The XRD test results indicate that Ni-Mo-SiC-TiN nanocomposite coatings has FCC structure, and all of them have a (111) preferred orientation. The increase of nanoparticle concentration reduces the crystallite size from 28.27 nm to 11.85 nm.

With the increase of SiC/TiN concentration to 20 g/L, the microhardness of the composite coating was increased to 561 HV, and the wear rate was reduced to 2.65×10^{-4} mm^3/N.m. The uniformly distributed nanoparticles play the role of bearing stress in the process of wear and the wear resistance of the coating is effectively improved.

Compared with Ni-Mo coating, the corrosion potential from -0.394 V to -0.250 V with the incorporation of nanoparticles, and the corrosion current density from 6.96 μA/cm^2 to 1.84 μA/cm^2. The uniformly dispersed SiC and TiN nanoparticles can reduce cracks and voids in the coating, effectively reduce the corrosion of the substrate coating by the etching solution.

It is very common to find SiC/TiN nanoparticles co-deposited to this preferential Ni (111) crystal face, but also a certain extent on the subordinate Ni (200) face. Thus it is deduced that the duplex nanoparticles deposited randomly to the matrix crystal faces during the pulse electrodeposition process. In addition, we also find that the duplex SiC/TiN particles can interact each other and promote the total deposition amount. The results show that the coating with SiC/TiN particle concentration of 20 g/L exhibits the best tribological properties and corrosion resistance.

Acknowledgment

The authors declare no conflict of interest. This work was financially supported by the Program of Study Abroad for Young Scholar sponsored by CSC (China Scholarship Council) (No. 201906565024), the National Natural Science Foundation of China (No. 51301021), the China Postdoctoral Science Foundation (No. 2016M592730), the Fundamental Research Funds for the Central Universities (No. 300102318205; 310831161020; 310831163401; 300102319304), the Innovation and Entrepreneurship Training Program of Chang' an University (No. 201910710144), the Key projects of Shaanxi Natural Science Foundation (2019JZ-27), and the Shaanxi Natural Science Basic Research Program-Shaanxi Coal (2019JLM-47).

References

[1] P.C. Huang, K.H. Hou, H.H. Sheu, M.D. Ger, G.L. Wang, Wear properties of Ni–Mo coatings produced by pulse electroforming, Surf. Coat. Technol. 258 (2014) 639-645. https://dx.doi.org/10.1016/j.surfcoat.2014.08.024.

[2] A. Lelevic, F.C. Walsh, Electrodeposition of NiP composite coatings: A review, Surf. Coat. Technol. 378 (2019) 124803. https://dx.doi.org/10.1016/j.surfcoat.2019.07.027.

[3] E. Beltowska-Lehman, A. Bigos, P. Indyka, M. Kot, Electrodeposition and characterisation of nanocrystalline Ni–Mo coatings, Surf. Coat. Technol. 211 (2012) 67-71. https://dx.doi.org/10.1016/j.surfcoat.2011.10.011.

[4] F. Xia, Q. Li, C. Ma, X. Guo, Preparation and characterization of Ni–AlN nanocoatings deposited by magnetic field assisted electrodeposition technique, Ceram. Int. 46 (2020) 2500–2509. https://dx.doi.org/10.1016/j.ceramint.2019.09.244.

[5] W. Xiong, M. Ma, J. Zhang, Y. Lian, The effects of Cr_2O_3 particles on the microstructure and wear-resistant properties of electrodeposited CoNiP coatings, Surf. Coat. Technol. 381 (2020): 125167. https://dx.doi.org/10.1016/j.surfcoat.2019.12516.

[6] T.R. Lee, L.w. Chang, C. Chen, Effect of electrolyte temperature on composition and phase structure of nanocrystalline Fe-Ni alloys prepared by direct current electrodeposition, Surf. Coat. Technol. 207 (2012) 523-528. https://dx.doi.org/10.1016/j.surfcoat.2012.07.069.

[7] Baosong. Li, Weiwei Zhang, Wen Zhang, Yuxing Huan, Preparation of Ni-W/SiC nanocomposite coatings by electrochemical deposition, J. Alloys Compd. 702 (2017) 38-50. https://dx.doi.org/10.1016/j.jallcom.2017.01.239

[8] T. Borkar, S.P Harimkar. Effect of electrodeposition conditions and reinforcement content on microstructure and tribological properties of nickel composite coatings, Surf. Coat. Technol. 205 (2011) 4124-4134. https://dx.doi.org/10.1016/j.surfcoat.2011.02.057

[9] A Rasooli, MS Safavi, F Babaei, Electrodeposited Ni–Fe–Cr_2O_3 nanocomposite coatings: A survey of influences of Cr_2O_3 nanoparticles loadings in the electrolyte, J. Alloys Compd. 822 (2020) 153725. https://dx.doi.org/10.1016/j.jallcom.2020.153725.

[10] K. Tsongas, D. Tzetzis, A. Karantzalis, G. Banias, D. Exarchos, D. Ahmadkhaniha, D. Bochtis, Microstructural, Surface Topology and Nanomechanical Characterization of Electrodeposited Ni-P/SiC Nanocomposite Coatings, Appl. Sci. 9(2019) 2901. https://dx.doi.org/10.3390/app9142901.

[11] Y. Zhou, F.Q. Xie, X.Q. Wu, W.D. Zhao, X. Chen, A novel plating apparatus for electrodeposition of Ni-SiC composite coatings using circulating-solution co-deposition technique, J. Alloys Compd. 699 (2017) 366-377. https://dx.doi.org/10.1016/j.jallcom.2016.12.331

[12] C.T.J. Low, R.G.A. Wills, F.C. Walsh, Electrodeposition of composite coatings containing nanoparticles in a metal deposit, Surf. Coat. Technol. 201 (2006) 371-383. https://dx.doi.org/10.1016/j.surfcoat.2005.11.123.

[13] I. Garcia, A. Conde, G. Langelaan, J.P. Celis, Improved corrosion resistance through microstructural modifications induced by codepositing SiC-particles with electrolytic nickel, Corros. Sci. 45 (2003) 1173-1189. https://dx.doi.org/10.1016/s0010-938x(02)00220-2.

[14] H.K. Lee, H.Y. Lee, J.M. Jeon, Codeposition of micro- and nano-sized SiC particles in the nickel matrix composite coatings obtained by electroplating, Surf. Coat. Technol. 201 (2007) 4711-4717. https://dx.doi.org/10.1016/j.surfcoat.2006.10.004.

[15] P. Narasimman, M. Pushpavanam, V.M. Periasamy, Wear and scratch resistance characteristics of electrodeposited nickel-nano and micro SiC composites, Wear. 292 (2012) 197-206. https://dx.doi.org/10.1016/j.wear.2012.05.009.

[16] M.D. Ger, Electrochemical deposition of nickel/SiC composites in the presence of surfactants, Mater. Chem. Phys. 87 (2004) 67-74. https://dx.doi.org/10.1016/j.matchemphys.2004.04.022.

[17] R. Sen, S. Bhattacharya, S. Das, K. Das, Effect of surfactant on the co-electrodeposition of the nano-sized ceria particle in the nickel matrix, J. Alloys Compd. 489 (2010) 650-658. https://dx.doi.org/10.1016/j.jallcom.2009.09.142.

[18] A. Hefnawy, N. Elkhoshkhany, A. Essam, Ni-TiN and Ni-Co-TiN composite coatings for corrosion protection: fabrication and electrochemical characterization, J. Alloy. Compd. 735 (2018) 600–606. https://dx.doi.org/10.1016/j.jallcom.2017.11.169.

[19] X.B. Zhu, C. Chao, G.Q. Zheng, Z. Zhang, J.F. Li, Electrodeposition and corrosion behavior of nanostructured Ni-TiN composite films, Trans. Nonferrous Met. Soc. China. 21 (2011) 2216-2224. https://dx.doi.org/10.1016/s1003-6326(11)60998-9.

[20] F.F. Xia, C. Liu, F. Wang, M.H. Wu, J.D. Wang, H.L. Fu, J.X. Wang, Preparation and characterization of Nano Ni-TiN coatings deposited by ultrasonic electrodeposition, J. Alloy. Compd. 490 (2010) 431-435. https://dx.doi.org/10.1016/j.jallcom.2009.10.026.

[21] M. Alizadeh, M. Mirak, E. Salahinejad, M. Alizadeh, M. Mirak, E. Salahinejad, M. Ghaffari, R. Amini, A. Roosta, Structural characterization of electro-codeposited Ni-Al_2O_3-SiC nanocomposite coatings, J. Alloy. Compd. 611 (2014) 161-166. https://dx.doi.org/10.1016/j.jallcom.2014.04.181.

[22] S. Dehgahi, R. Amini, M. Alizadeh, Microstructure and corrosion resistance of Ni-Al_2O_3-SiC nanocomposite coatings produced by electrodeposition technique, J. Alloy. Compd. 692 (2017) 622-628. https://dx.doi.org/10.1016/j.jallcom.2016.08.244.

[23] S. Dehgahi, R. Amini, M. Alizadeh. Corrosion, passivation and wear behaviors of electrodeposited Ni-Al_2O_3-SiC nano-composite coatings, Surf. Coat. Technol. 304 (2016) 502-511. https://dx.doi.org/10.1016/j.surfcoat.2016.07.007.

[24] S.R. Ardakani, A. Afshar, S. Sadreddini, A.A. Ghanbari, Characterization of Ni-P-SiO_2-Al_2O_3 nanocomposite coatings on aluminum substrate, Mater. Chem. Phys. 189 (2017) 207-214. https://dx.doi.org/10.1016/j.matchemphys.2016.12.023.

[25] W. Zhang, B. Li, C. Ji, Synthesis and characterization of Ni-W/TiN nanocomposite coating with enhanced wear and corrosion resistance deposited by pulse electrodeposition, Ceram. Int. 45 (2019) 14015-14028. https://dx.doi.org/10.1016/j.ceramint.2019.04.101.

[26] A.R. Shetty, A.C. Hegde, Effect of TiO_2 on electrocatalytic behavior of Ni-Mo alloy coating for hydrogen energy, Materials Science for Energy Technologies. 1 (2018) 97-105. https://dx.doi.org/10.1016/j.mset.2018.06.003.

[27] A. Laszczyńska, J. Winiarski, B. Szczygieł, I. Szczygieł, Electrodeposition and character-ization of Ni–Mo–ZrO_2 composite coatings, Appl. Surf. Sci. 369 (2016) 224–231. https://doi.org/10.1016/j.apsusc.2016.02.086.

[28] Y.K. Xu, S. Ma, M.Y Fan, Y.N. Chen, X.D Song, J.M. Hao, Design and properties investigation of Ni-Mo composite coating reinforced with duplex nanoparticles, Surf. Coat. Technol. 363 (2019) 51-60. https://dx.doi.org/10.1016/j.surfcoat.2019.02.016.

[29] A. Morteza, S. Hamed, Characterization of Ni-Cu matrix, Al_2O_3, reinforced nanocomposite coatings prepared by electrodeposition, Appl. Surf. Sci. 456 (2018) 195-203. https://dx.doi.org/10.1016/j.apsusc.2018.06.095.

[30] S.K. Ghosh, A.K. Grover, G.K. Dey, M.K. Totlani, Nanocrystalline Ni-Cu alloy plating by pulse electrolysis, Surf. Coat. Technol. 126 (2000) 48–63. https://dx.doi.org/10.1016/s0257-8972(00)00520-x.

[31] S. Mirzamohammadi, H. Khorsand, M. Aliofkhazraei, D.V. Shtansky, Effect of carbamide concentration on electrodeposition and tribological properties of Al_2O_3 nanoparticle reinforced nickel nanocomposite coatings, Tribol. Int. 117 (2018) 68-77. https://dx.doi.org/10.1016/j.triboint.2017.08.003.

[32] E.A. Pavlatou, M. Stroumbouli, P. Gyftou, N. Spyrellis, Hardening effect induced by incorporation of SiC particles in nickel electrodeposits, J. Appl. Electrochem. 36 (2006) 385-394. https://dx.doi.org/10.1007/s10800-005-9082-y.

[33] J. Ehrhardt, Composite electroplating by using brush technique, Ind. Eng. Chem. Prod. Res. Dev. 24 (4) (1985) 575–578, https://doi.org/10.1021/i300020a016.

[34] H. Gül, F. Kılıç, M. Uysal, S. Aslan, A. Alp, H. Akbulut, Effect of particle concentration on the structure and tribological properties of submicron particle SiC reinforced Ni metal matrix composite (MMC) coatings produced by electrodeposition, Appl. Surf. Sci. 258 (2012) 4260-4267. https://dx.doi.org/10.1016/j.apsusc.2011.12.069.

[35] M.R. Vaezi, S.K. Sadrnezhaad, L. Nikzad, Electrodeposition of Ni–SiC nano-composite coatings and evaluation of wear and corrosion resistance and electroplating characteristics, Colloids Surf. A. 315 (2008) 176-182. https://dx.doi.org/10.1016/j.colsurfa.2007.07.027.

[36] B. Bakhit, A. Akbari, F. Nasirpouri, M.G. Hosseini, Corrosion resistance of Ni-Co alloy and Ni-Co/SiC nanocomposite coatings electrodeposited by sediment codeposition technique, Appl. Surf. Sci. 307 (2014): 351-359. https://dx.doi.org/10.1016/j.apsusc.2014.04.037.

[37] B. Bakhit, A. Akbari, Effect of particle size and co-deposition technique on hardness and corrosion properties of Ni–Co/SiC composite coatings, Surf. Coat. Technol. 206 (2012) 4964-4975. https://dx.doi.org/10.1016/j.surfcoat.2012.05.122.

[38] X.H. Chen, C.S. Chen, H.N. Xiao, F.Q. Cheng, G. Zhang, G.J. Yi, Corrosion behavior of carbon nanotubes/Ni composite coating, Surf. Coat. Technol. 191 (2005) 351-356. https://dx.doi.org/10.1016/j.surfcoat.2004.04.055.

[39] N. Guglielmi, Kinetics of the deposition inert particles from electrolytic baths, J. Electrochem. Soc. 119 (1972) 1009-1012. https://dx.doi.org/10.1149/1.2404383.

[40] J.P. Celis, J.R. Roos, C. Buelens, A mathematical model for the electrolytic codeposition of particles with a metallic matrix, J. Electrochem. Soc. 134 (1987) 1402-1408. https://dx.doi.org/10.1149/1.2100680.

[41] B. Bakhit, A. Akbari. Synthesis and characterization of Ni–Co/SiC nanocomposite coatings using sediment co-deposition technique, J. Alloys Compd. 560 (2013): 92-104. http://dx.doi.org/10.1016/j.jallcom.2013.01.122.

[42] A. Lelevic, F.C. Walsh, Electrodeposition of NiP composite coatings: A review, Surf. Coat. Technol. 378 (2019) 124803. https://doi.org/10.1016/j.surfcoat.2019.07.027.

[43] J. Foster, B. Cameron, The effect of current density and agitation on the formation of electrodeposited composite coatings, Trans. IMF. 1 (1976): 178-183. https://dx.doi.org/10.1080/00202967.1976.11870395.

[44] N.A. Polyakov, Y.M. Polukarov, V. N. Kudryavtsev, Electrodeposition of composite chromium coatings from Cr (III) sulfate-oxalate solution suspensions containing Al_2O_3, SiC, Nb_2N, and Ta_2N particles. Prot. Met. Phys. Chem. Surf. 46 (2010) 75-81. https://dx.doi.org/10.1134/s2070205110010119.

[45] Z.N. Wing, TiN modified SiC with enhanced strength and electrical properties, J. Eur. Ceram. Soc. 37 (2017) 1373-1378. https://dx.doi.org/10.1016/j.jeurceramsoc.2016.11.007.

[46] N. Periene, A. Cesuniene, E. Matulionis, Codeposition of mixtures of dispersed particles with nickel-phosphorus electrodeposits. Plat. Surf. Finish. 10 (1994): 68-81.

[47] Y. Zhou, F.Q. Xie, X.Q. Wu, W.D. Zhao, X. Chen, A novel plating apparatus for electrodeposition of Ni-SiC composite coatings using circulating-solution co-deposition technique. J. Alloys Compd. 699 (2017) 366-377. http://dx.doi.org/10.1016/j.jallcom.2016.12.331

[48] J. Foster, B. Cameron, The effect of current density and agitation on the formation of electrodeposited composite coatings, Trans. IMF. 54 (1976) 178-183. https://doi.org/10.1080/00202967.1976.11870395

[49] B. Li, W. Zhang, T. Mei, Y. Miao, Fabrication of Ni–B/TiC-Y2O3 nanocomposites by one-step electrodeposition at different duty cycle and evaluation of structural, surface and performance as protective coating. J. Alloys Compd. 823 (2020) 153888. https://doi.org/10.1016/j.jallcom.2020.153888.

Tables

Table Ⅰ Electrolyte composition and operating parameters of Ni-Mo-SiC-TiN composite coating prepared by pulse electrodeposition.

Electrolyte composition and electrodeposition parameters	
Electrolyte component	Concentration (g·L^{-1})
Nickel sulphate ($NiSO_4 \cdot 6H_2O$)	52.6
Sodium molybdate ($Na_2MoO_4 \cdot 2H_2O$)	1.452
Sodium citrate ($Na_3C_6H_5O_7 \cdot 2H_2O$)	88.2
Ammonium chloride (NH_4Cl)	27
Sodium dodecyl sulfate (SDS)	0.1
SiC particles	0, 2, 4, 6, 8, 10, 12
TiN particles	0, 2, 4, 6, 8, 10, 12
Operating parameters for composite coatings	
Temperature (℃)	50
Plating time (min)	20
Magnetic stirring rate (rpm)	350
Current density (A·dm^{-2})	8
Duty cycle (%)	20
Pulse frequency (Hz)	1000

Table Ⅱ the corrosion parameters for Ni-Mo-SiC-TiN composite coating with different nanoparticles concentration.

Nano-particles concentration (SiC+TiN) in the bath (g/L)	βa (mv/decade)	βc (mv/decade)	I_{corr} (μA/cm^2)	E_{corr} (V)	R_p (Ω·cm^2)
0	24.4	38.9	6.96	-0.394	935
4	27.8	34.5	5.66	-0.361	1181
8	24.4	29.5	4.78	-0.349	1370
12	34.0	34.5	3.10	-0.324	2399
16	33.8	32.5	2.19	-0.294	3285
20	33.3	32.6	1.84	-0.250	3887
24	34.6	32.4	2.01	-0.266	3615

Figure captions

Fig. 1. (a, b) SEM morphologies of Ni-Mo composite coating; (c-h) SEM morphologies of Ni-Mo-SiC-TiN composite coatings prepared by the electrolytes with a series of SiC and TiN concentrations of 4, 8, 12, 16, 20, and 24 g/L.

Fig. 2. LSCM 3D morphologies of Ni-Mo-SiC-TiN composite coatings prepared by the electrolytes with different SiC and TiN concentrations of 0, 8, 16, and 20 g/L, respectively.

Fig. 3. Cross-sectional SEM micrograph of the Ni-Mo coating and Ni-Mo-SiC-TiN nanocomposite coating with different nanoparticles concentrations; and the cross-section of each coating with higher magnification is exhibited at the lower position.

Fig. 4. (a) XRD patterns of the TiN and SiC nanoparticles; (b) XRD patterns of Ni-Mo coating and Ni-Mo-SiC-TiN composite coatings; (c) average crystallite size D; (d) nanoparticle and Mo content in the deposited composite coatings.

Fig. 5. EDS elemental mapping of Ni-Mo-SiC-TiN nanocomposite coating prepared by the electrolytes with nanoparticles concentrations of 20 g/L under TEM bright imaging.

Fig. 6. (a) Microhardness and wear rate of the Ni-Mo coating and Ni-Mo-SiC-TiN composite coating prepared with different nanoparticle concentrations; (b) Friction coefficients.

Fig. 7. (a-d) the SEM and 3D morphology of the worn surface was prepared in an electrolyte with different nanoparticle concentrations; (e) the wear schematic diagram of Ni-Mo coating and Ni-Mo-SiC-TiN nanocomposite coatings.

Fig. 8. (a) The polarization curves of Ni-M-SiC-TiN at different concentration of nanoparticles; (b-e) SEM image of samples after polarization experiment.

Fig. 9. (a, d) TEM image of Ni-Mo-SiC-TiN nanocomposite coating; (b) SAED of the matrix; (c) SAED image of the red gridlines in (a); (e) HR-TEM image of the red gridlines in (d); (f)

HR-TEM image of the red gridlines in (a); (g) schematic illustration of the particle incorporation mechanism; (h) the formation of a protrusion cluster and gap structure.

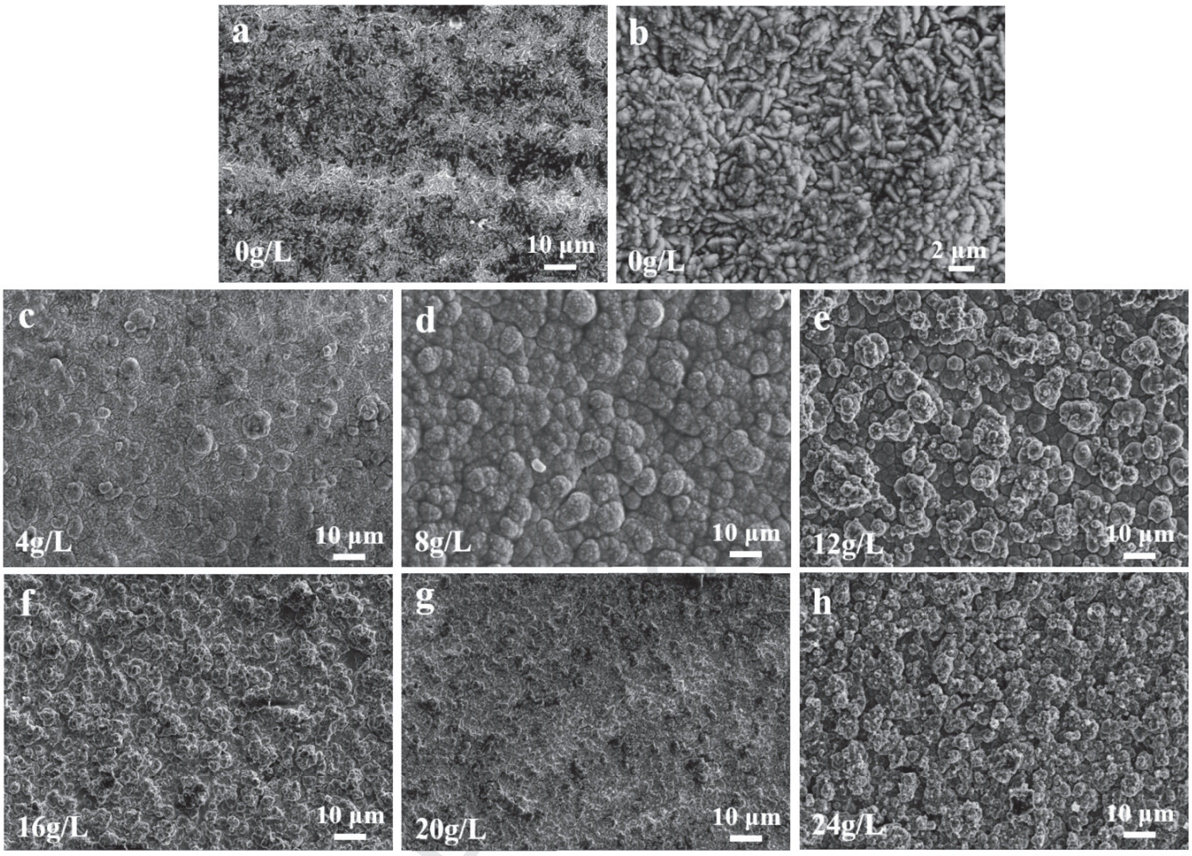
a
0g/L
10 µm
b
0g/L
2 µm
c
4g/L
10 µm
d
8g/L
10 µm
e
12g/L
10 µm
f
16g/L
10 µm
g
20g/L
10 µm
h
24g/L
10 µm

1

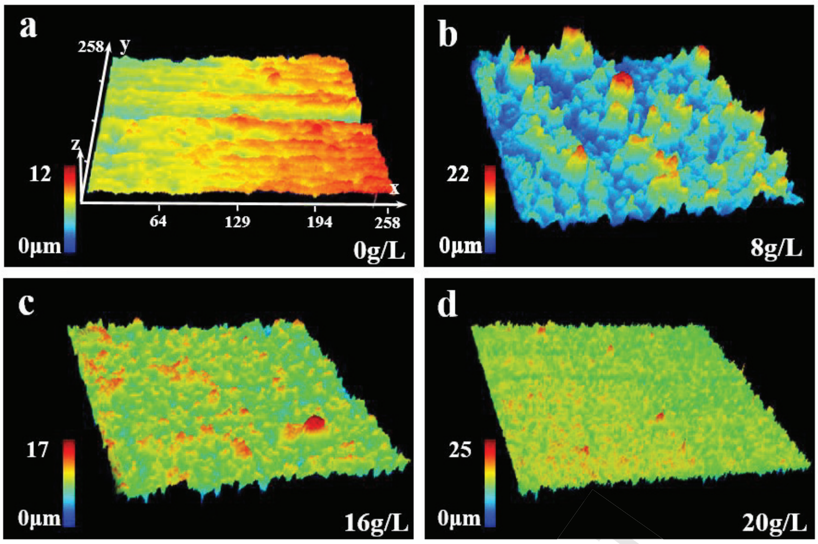
a
258
y
z
12
0μm
x
64
129
194
258
0g/L
b
22
0μm
8g/L
c
17
0μm
16g/L
d
25
0μm
20g/L

2

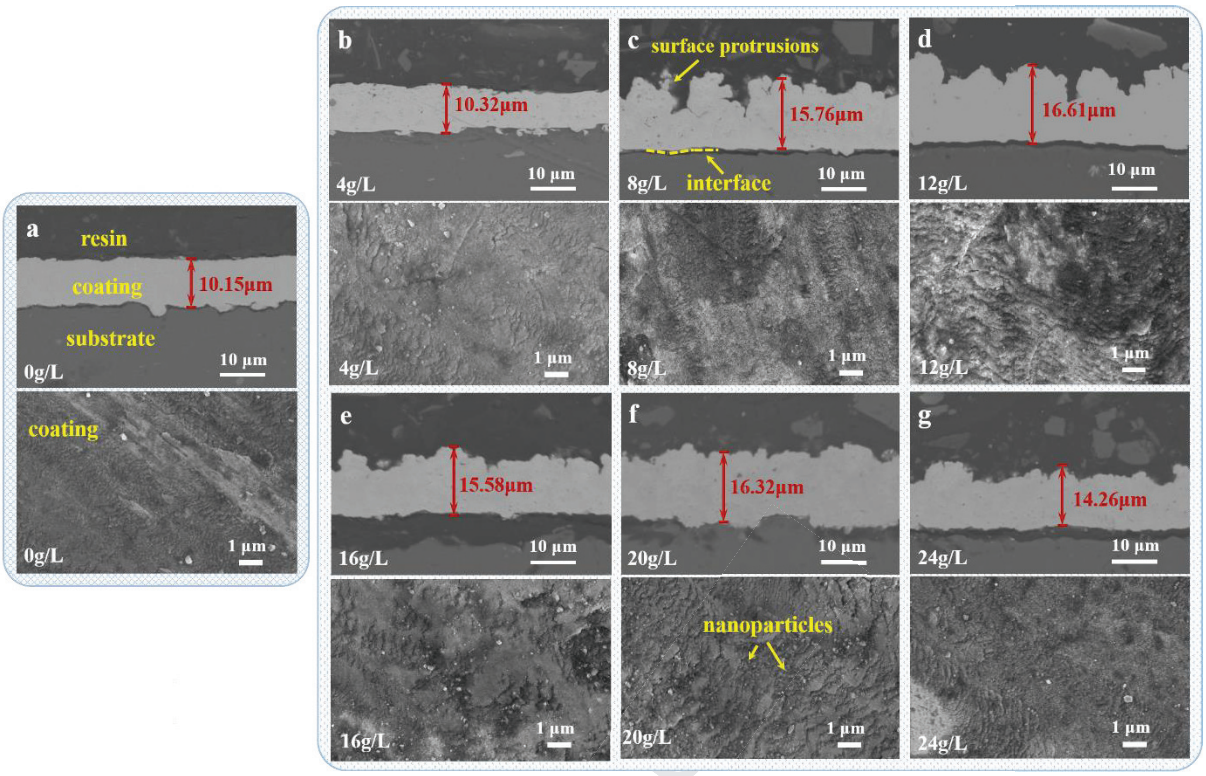
a
resin
coating
10.15μm
substrate
0g/L
10 μm
coating
0g/L
1 μm
b
10.32μm
4g/L
10 μm
4g/L
1 μm
c
surface protrusions
15.76μm
8g/L
interface
10 μm
8g/L
1 μm
d
16.61μm
12g/L
10 μm
12g/L
1 μm
e
15.58μm
16g/L
10 μm
16g/L
1 μm
f
16.32μm
20g/L
10 μm
nanoparticles
20g/L
1 μm
g
14.26μm
24g/L
10 μm
24g/L
1 μm

3

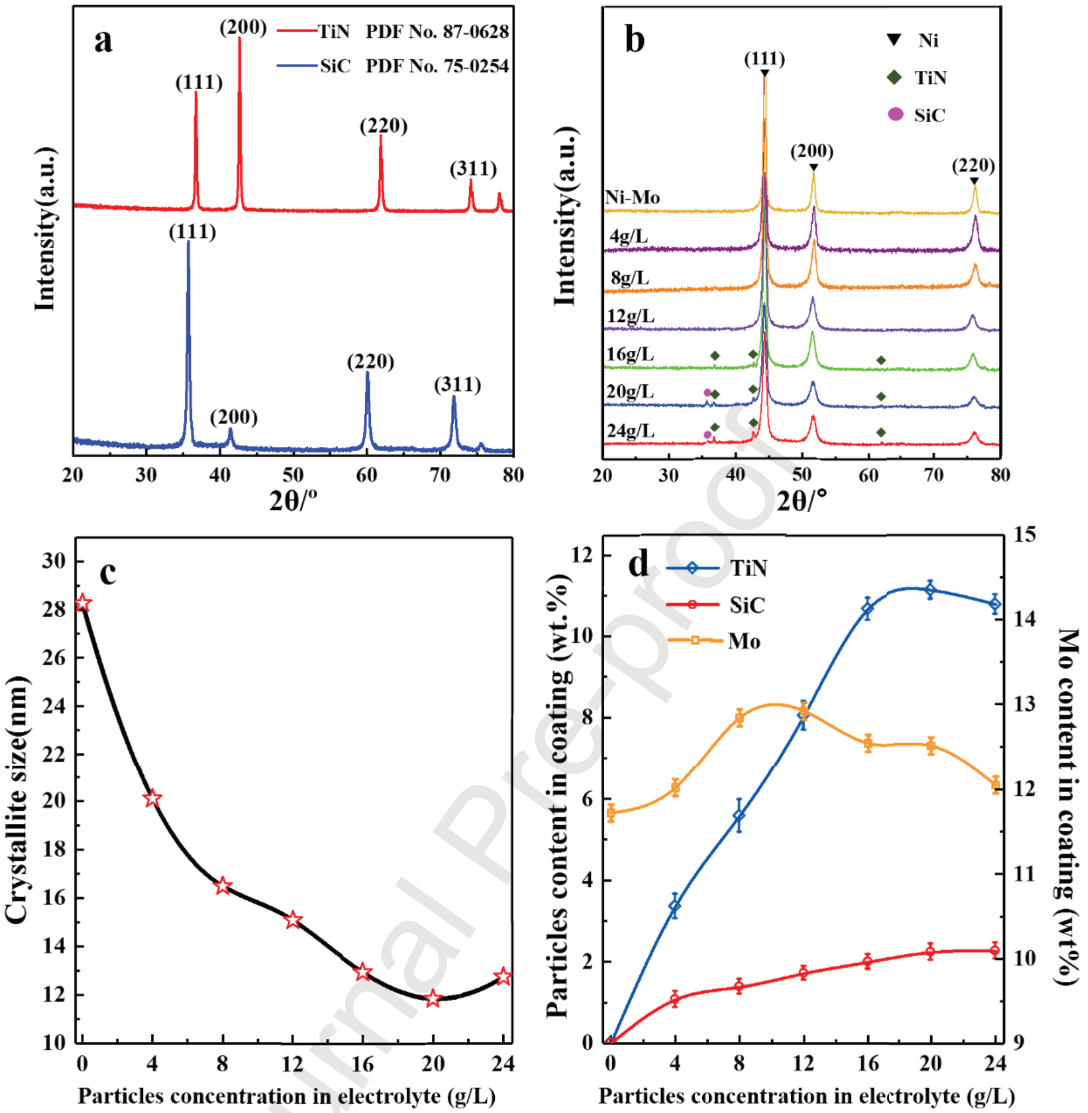
a
(200)
TiN PDF No. 87-0628
SiC PDF No. 75-0254
(111)
(220)
(311)
(111)
(220)
(200)
(311)
Intensity(a.u.)
20 30 40 50 60 70 80
2θ/°
b
▼ Ni
◆ TiN
● SiC
(111)
(200)
(220)
Ni-Mo
4g/L
8g/L
12g/L
16g/L
20g/L
24g/L
Intensity(a.u.)
20 30 40 50 60 70 80
2θ/°
c
Crystallite size(nm)
10 12 14 16 18 20 22 24 26 28 30
0 4 8 12 16 20 24
Particles concentration in electrolyte (g/L)
d
TiN
SiC
Mo
Particles content in coating (wt.%)
0 2 4 6 8 10 12
Mo content in coating (wt%)
9 10 11 12 13 14 15
0 4 8 12 16 20 24
Particles concentration in electrolyte (g/L)

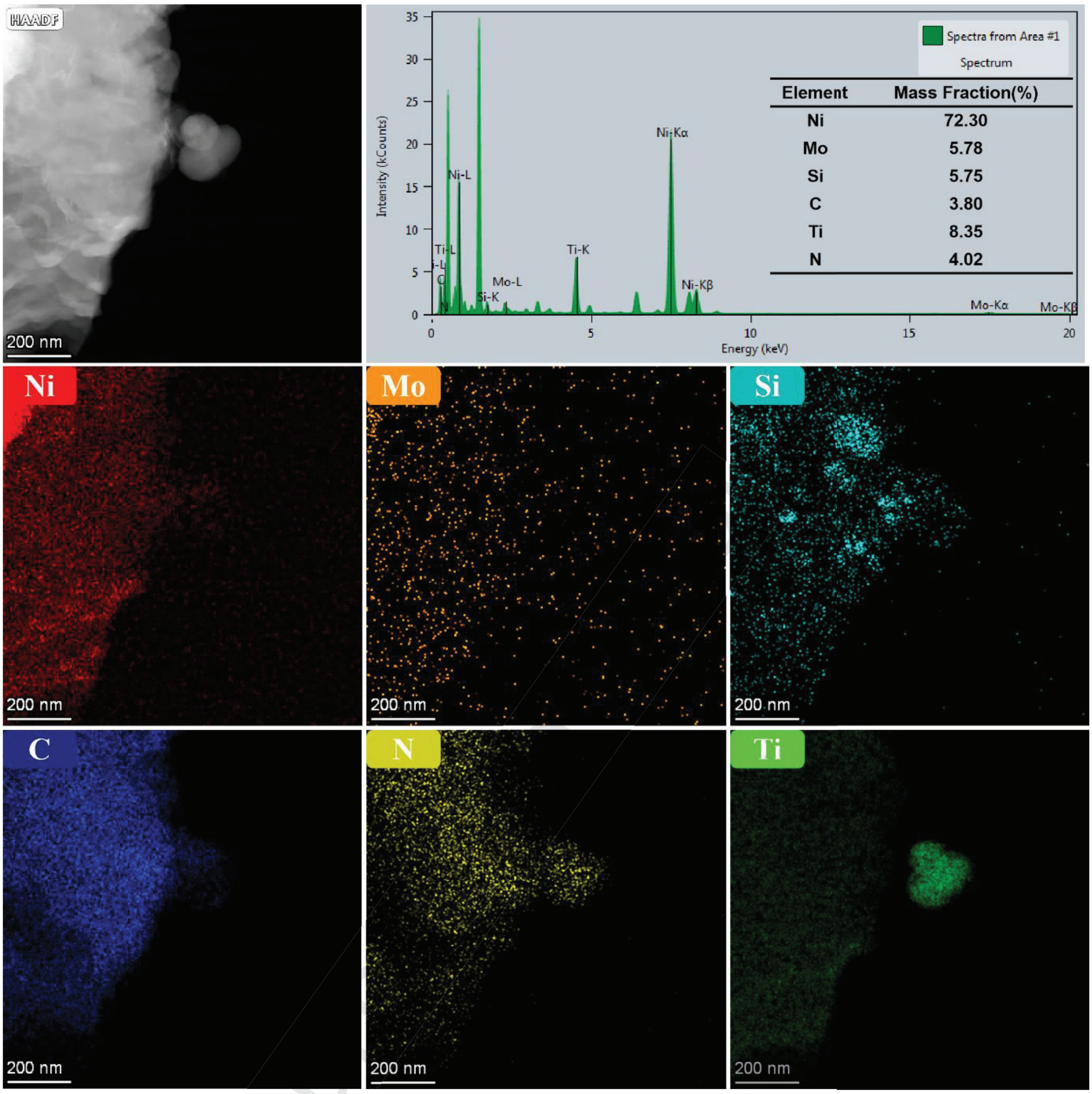

Element	Mass Fraction(%)
Ni	72.30
Mo	5.78
Si	5.75
C	3.80
Ti	8.35
N	4.02

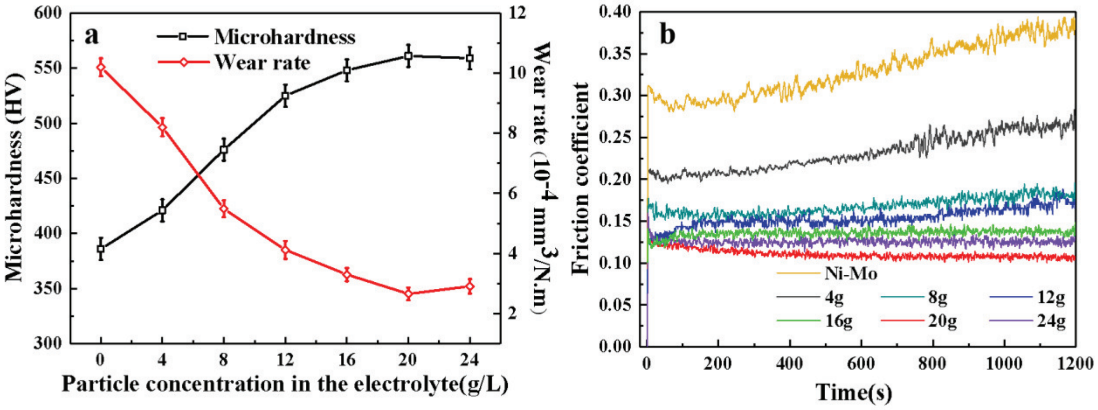
a
Microhardness
Wear rate
Microhardness (HV)
600
550
500
450
400
350
300
Wear rate (10^{-4} mm^3/N.m)
12
10
8
6
4
2
0
4
8
12
16
20
24
Particle concentration in the electrolyte(g/L)
b
Friction coefficient
0.40
0.35
0.30
0.25
0.20
0.15
0.10
0.05
0.00
Ni-Mo
4g
8g
12g
16g
20g
24g
0
200
400
600
800
1000
1200
Time(s)

6

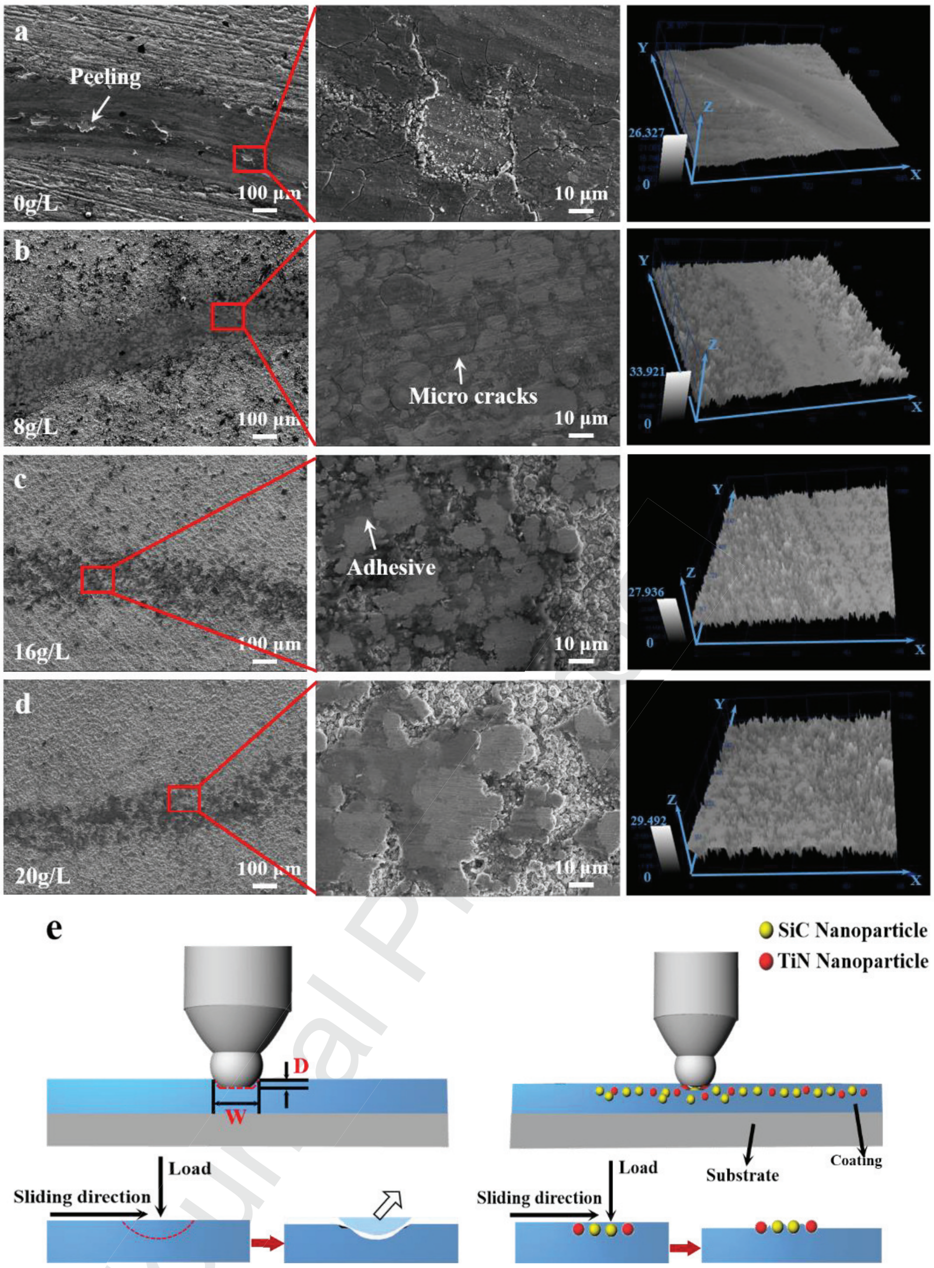
a
Peeling
100 µm
0g/L
10 µm
Y
Z
X
26.327
0
b
Micro cracks
100 µm
8g/L
10 µm
33.921
0
c
Adhesive
100 µm
16g/L
10 µm
27.936
0
d
100 µm
20g/L
10 µm
29.492
0
e
SiC Nanoparticle
TiN Nanoparticle
D
W
Load
Sliding direction
Substrate
Coating

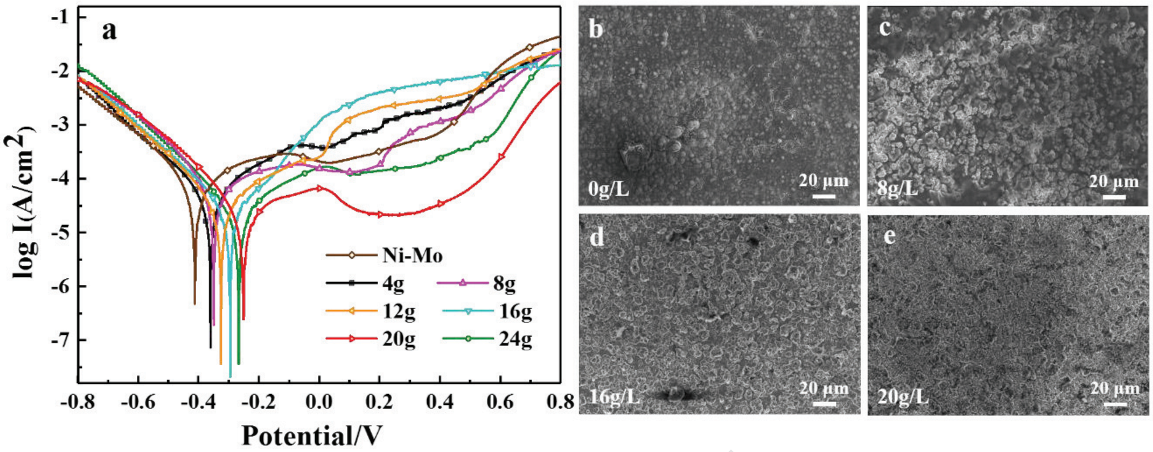
a
log I(A/cm^2)
-1
-2
-3
-4
-5
-6
-7
-0.8
-0.6
-0.4
-0.2
0.0
0.2
0.4
0.6
0.8
Potential/V
Ni-Mo
4g
8g
12g
16g
20g
24g
b
0g/L
20 µm
c
8g/L
20 µm
d
16g/L
20 µm
e
20g/L
20 µm

8

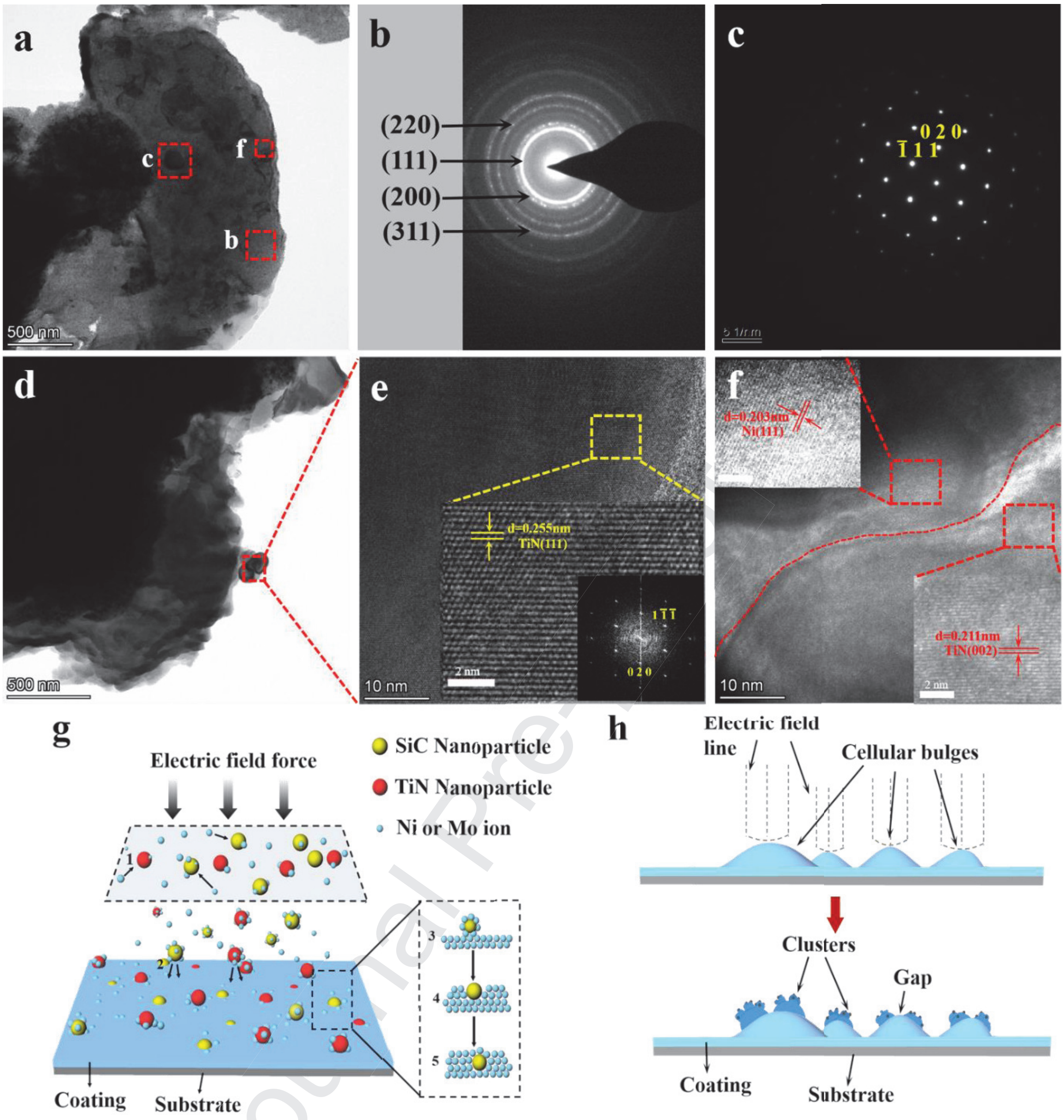
a
c
f
b
500 nm
b
(220)
(111)
(200)
(311)
c
0 2 0
1̄ 1 1
5 1/nm
d
500 nm
e
d=0.255nm
TiN(111)
1 1̄ 1̄
0 2 0
2 nm
10 nm
f
d=0.203nm
Ni(111)
d=0.211nm
TiN(002)
2 nm
10 nm
g
Electric field force
SiC Nanoparticle
TiN Nanoparticle
Ni or Mo ion
1
2
3
4
5
Coating
Substrate
h
Electric field
line
Cellular bulges
Clusters
Gap
Coating
Substrate